Supplementary Figures for The Linked Selection Signature of Rapid Adaptation in Temporal Genomic Data

Vince Buffalo[*,†,1] and Graham Coop[†]

[*]Population Biology Graduate Group
[†]Center for Population Biology, Department of Evolution and Ecology, University of California, Davis, CA 95616
[1]Email for correspondence: vsbuffalo@ucdavis.edu

September 25, 2019

1 Validation of simulation routine

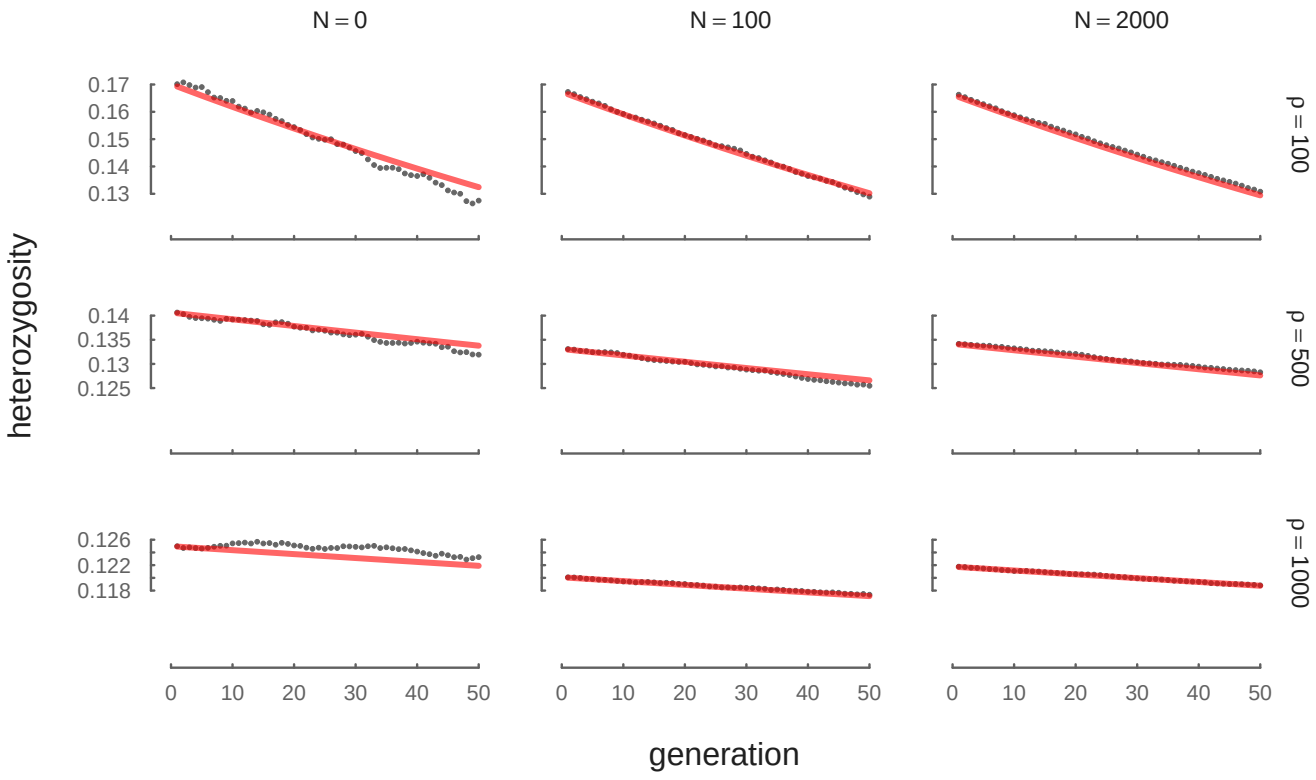

Figure 1.1: The neutral decay of heterozygosity due to drift, averaged across 100 replicates and a variety of N and ρ levels. The red line is the theoretical expectation $H_t = H_1(1 - 1/(2N))^{t-1}$.

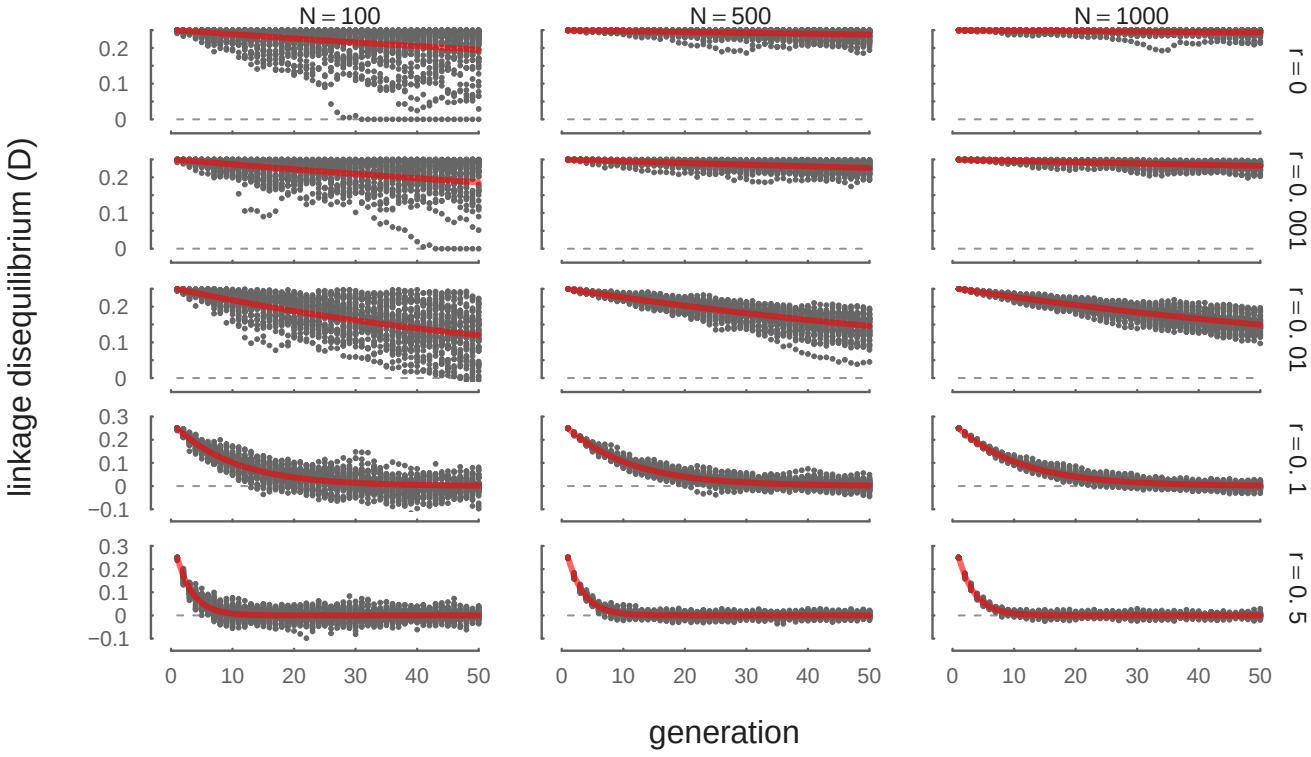

Figure 1.2: The decay of LD between neutral sites due to recombination, across 100 replicates and a variety of V_A and R levels. The initial population is created to have an artificial level of initial LD, with half the gametes carrying all derived alleles, and the other half carrying all ancestral alleles. The red line is the theoretical expectation $D_t = D_1(1 - 1/(2N))^{t-1}(1 - r)^{t-1}$.

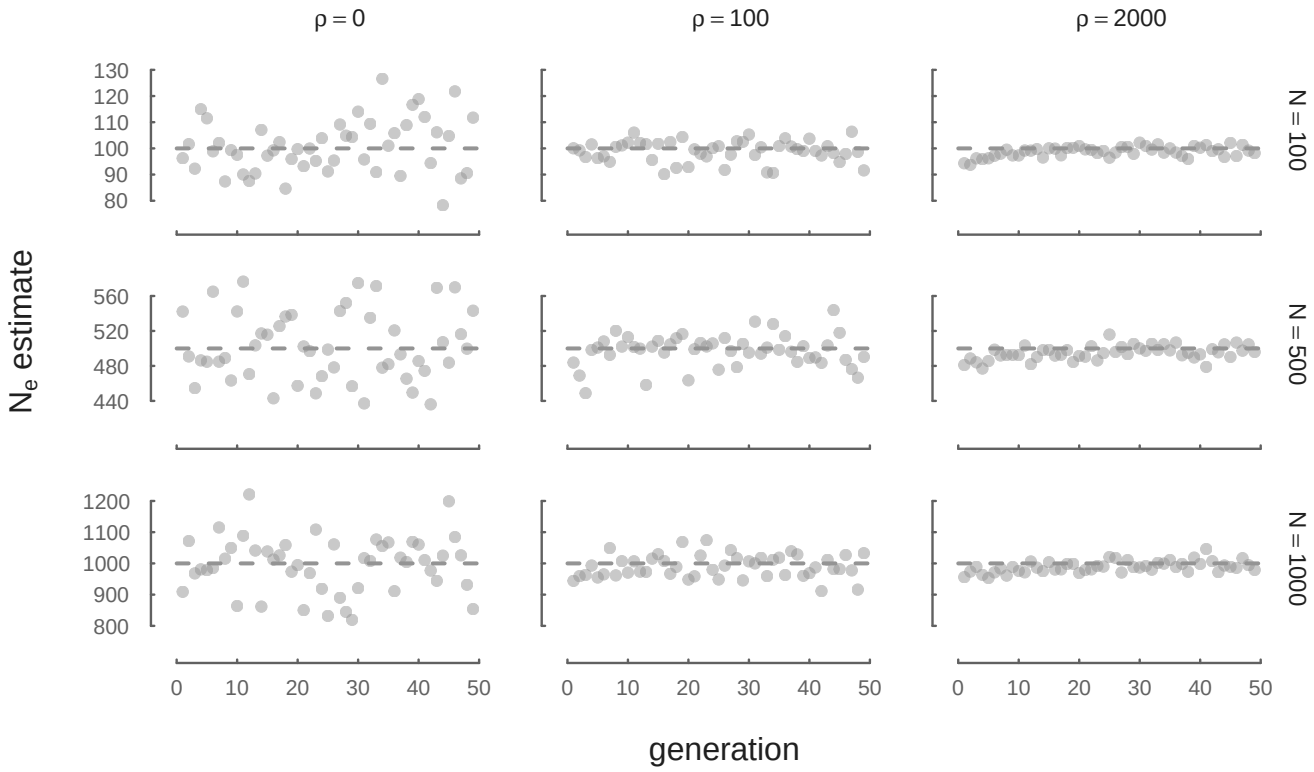

Figure 1.3: N_e estimated through time from neutral forward simulations is consistent with true N across a variety of recombination ρ and N parameters. Here, we estimate N_e with $\widehat{N_e} = {}^{p(1-p)}/_{2\,\mathrm{Var}(\Delta p)}$ from neutral allele frequency changes.

2 Dynamics of Variances

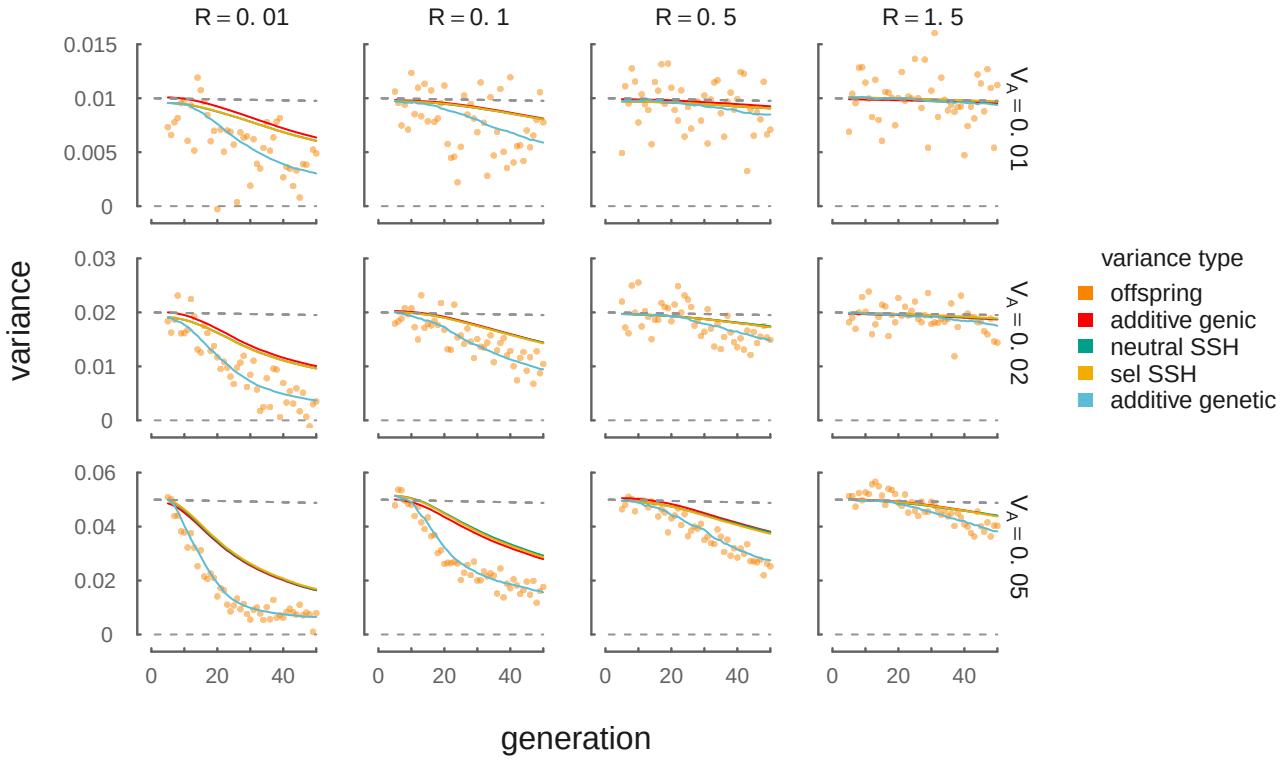

Figure 2.1: The dynamics of different variances in our simulations, across a variety of initial target V_A and R levels. Orange points represent the empirical heritable variance in offspring (e.g. with the noise of the Wright–Fisher reproduction process removed). These closely track the additive genetic variance for the trait undergoing directional selection, $V_A = \mathrm{Var}(z)$. The red line shows the dynamics of additive genic variance, $V_a = 2\sum_l \alpha_l^2 p_l(1-p_l)$, which is closely tracked by both the selected (yellow line) and neutral (green line) sum of site heterozygosity proxies described in Section 2.3.

3 Supplementary Temporal Autocovariance Figures

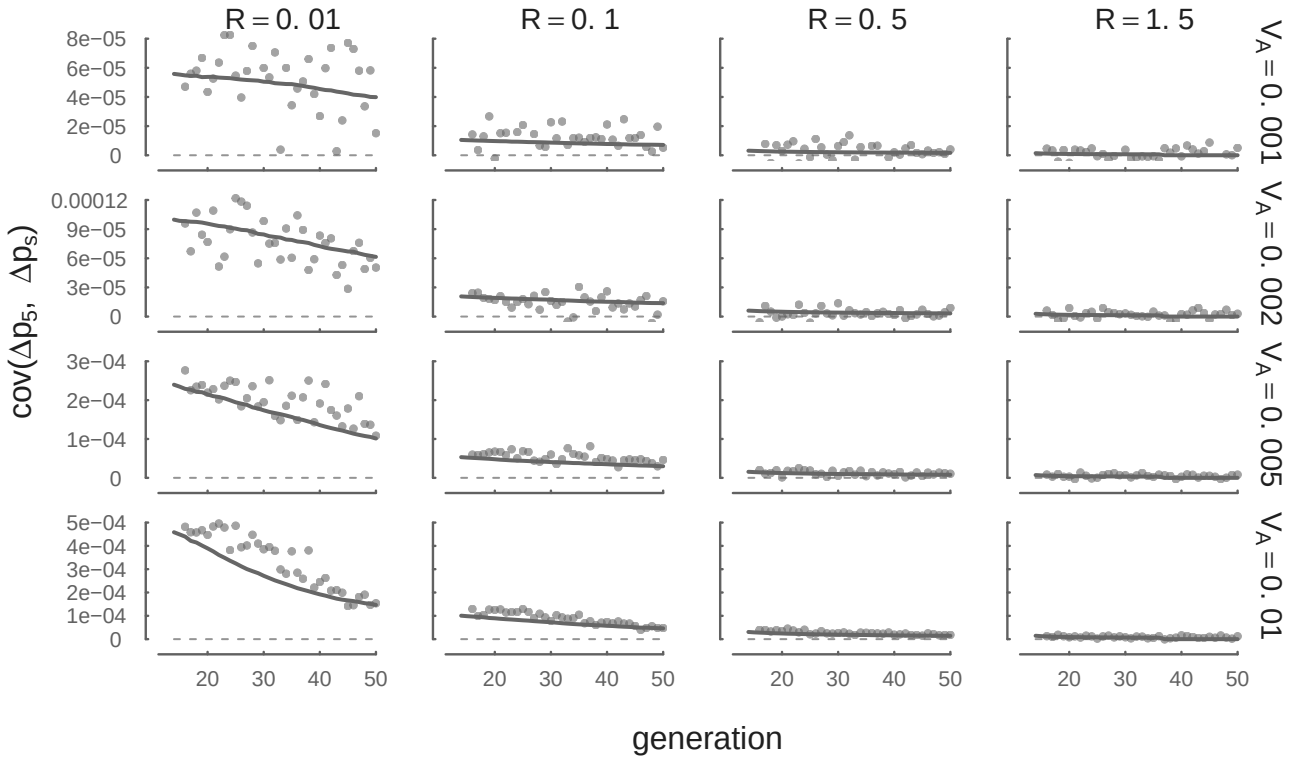

Figure 3.1: Each panel shows the temporal autocovariance $\mathrm{Cov}(\Delta p_{13}, \Delta p_s)$ on the y-axis, where s varies along the x-axis. This is analogous to Figure 2 with a different reference generation ($t = 13$), and compares the averaged simulation results (points) with the temporal autocovariance predicted by Equation (10) using the empirical additive genetic variance (curve). The covariances in these panels are weaker compared to those in Figure 2 because by generation 13, additive genetic variance for fitness and the linkage disequilibria between neutral and selected sites has decayed.

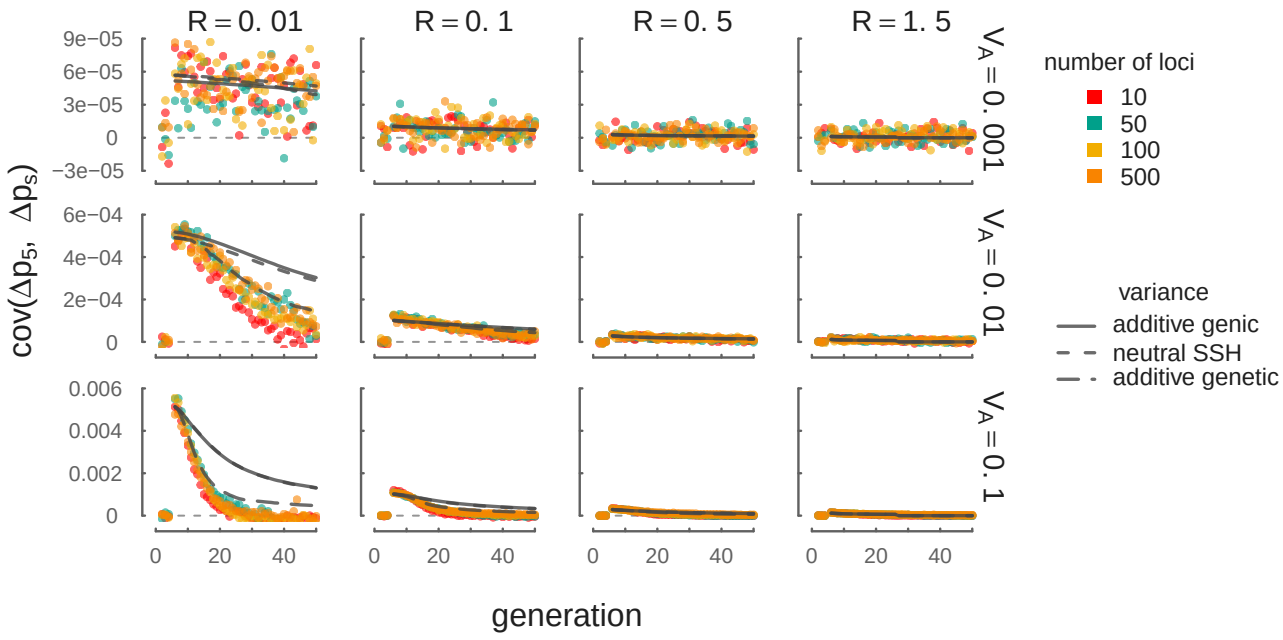

Figure 3.2: A version of Figure 2 with a subset of V_A parameters used in our simulations that vary over orders of magnitude. This demonstrates that our theory using the empirical additive genic variance (solid gray line), additive genetic variance (long dashed gray line), and the neutral SSH proxy (short dashed gray lines) performs as described in Section 2.5 even when V_A varies over orders of magnitude in a region. Higher variance in the empirical covariances with weak selection ($V_A = 0.001$) are due to chance covariances due to drift. The light gray dashed line depicts $\text{Cov}(\Delta p_5, \Delta p_s) = 0$.

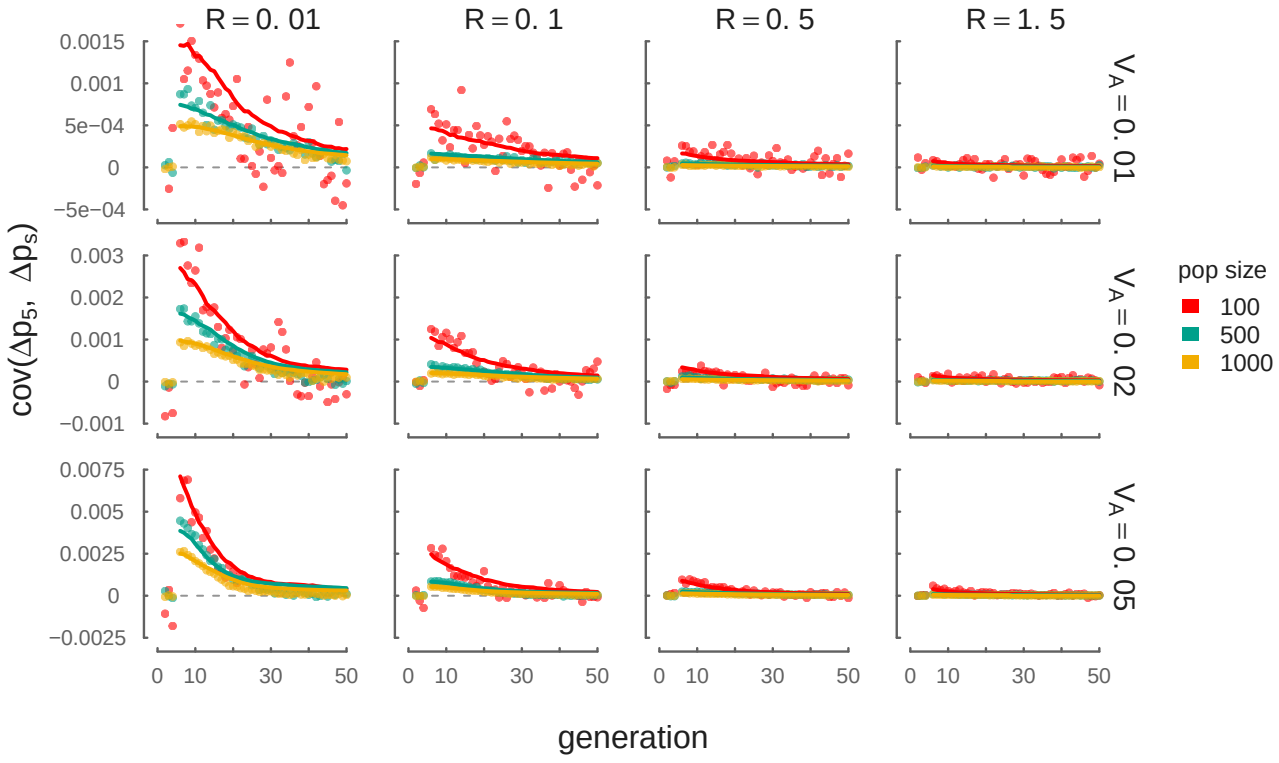

Figure 3.3: A version of Figure 2 demonstrating temporal autocovariance simulation results and theoretical predictions with varying N. This demonstrates that our theory using the empirical additive genetic variance (lines) fits simulations across a variety of N parameters. The light gray dashed line depicts $\text{Cov}(\Delta p_5, \Delta p_s) = 0$. Note that the initial LD varies due to differing equilibrium levels of LD from our burnin across varying N.